The Amyloid β Peptide ($A\beta_{1-40}$) Is Thermodynamically Soluble at Physiological Concentrations[†]

Parijat Sengupta,[‡] K. Garai,[‡] B. Sahoo,[‡] Yuan Shi,[§] David J. E. Callaway,[§] and S. Maiti*,[‡]

Department of Chemical Sciences, Tata Institute of Fundamental Research, Homi Bhabha Road, Colaba, Mumbai 400005, India, and Center for Neurosciences, North Shore/LIJ Research Institute, 350 Community Drive, Manhasset, New York 11030-3849

Received January 27, 2003; Revised Manuscript Received June 13, 2003

ABSTRACT: Precipitation of the 39−43-residue amyloid β peptide (Aβ) is a crucial factor in Alzheimer's disease (AD). In normal as well as in AD-afflicted brain, the Aβ concentration is estimated to be a few nanomolar. Here we show that $A\beta_{1-40}$ precipitates *in vitro* only if the dissolved concentration is >14 μM. Using fluorescence correlation spectroscopy, we further show that the precipitation is complete in 1 day, after which the size distribution of Aβ monomer/oligomers in the solution phase becomes stationary in time and independent of the starting Aβ concentration. Mass spectra confirm that both the solution phase and the coexisting precipitate contain chemically identical Aβ molecules. Incubation at 68 °C for 1 h reduces the solubility by <12%. Together, these results show that the thermodynamic saturation concentration (C_{sat}) of $A\beta_{1-40}$ in phosphate-buffered saline (PBS) at pH 7.4 has a well-defined lower limit of 15.5 ± 1 μM. Divalent metal ions (believed to play a role in AD) at near-saturation concentrations in PBS reduce C_{sat} only marginally (2 mM Mg^{2+} by 6%, 2.5 μM Ca^{2+} by 7%, and 4 μM Zn^{2+} by 11%). Given that no precipitation is possible at concentrations below C_{sat}, we infer that coprecipitant(s), and not properties of $A\beta_{1-40}$ alone, are key factors in the *in vivo* aggregation of Aβ.

Alzheimer's disease (AD)[1] (*1*) is the most common age-related neurodegenerative disorder. This irreversible disorder is caused by neuronal death, resulting in the impairment of cognitive functions. Clinical investigations as well as experiments on animal models suggest that the primary agent of the neuronal death is a 39−43-amino acid polypeptide known as amyloid β peptide (henceforth called Aβ) (*2*−*4*). Aβ is a natural component of cerebro spinal fluid (CSF) and blood plasma, and is soluble under normal conditions (*5*−*7*). In a diseased brain, it forms insoluble β-sheet-rich (*8*, *9*) fibrillar plaques and diffusible aggregates which are cytotoxic (*10*−*12*). Therefore, when and why Aβ loses its solubility and how external agents may influence this process are intensely studied questions.

The concentration below which a solute does not precipitate is known as the equilibrium or thermodynamic saturation concentration (C_{sat}) of the solute. However, even when the concentration of the solute is above C_{sat}, it may not necessarily precipitate within a finite time. Kinetic traps [which may be "on" or "off" the pathway toward precipitation (*13*)] or kinetic barriers [such as a "nucleation" barrier (*14*, *15*)] may indefinitely delay precipitation. An external agent that influences aggregation may act either by modulating the kinetic traps or barriers or by changing the thermodynamic solubility (or both). It is thus important to have a quantitative understanding of both.

The *in vivo* concentration of Aβ in the CSF of a normal brain is estimated to be in the low nanomolar range, and it is not significantly higher in a diseased brain (*5*−*7*). This has been taken to indicate that Aβ can aggregate at approximately nanomolar concentrations, and its aggregation is kinetically limited. In fact, epidemiology of Huntington's chorea, another closely related protein aggregation disease, suggests nucleation-limited growth as the most consistent explanation for the observed progression of the disease (*15*). *In vitro* studies of aggregation have thus largely focused on the kinetics of precipitation of pure Aβ in a supersaturated solution. Concentrations in the range of tens to hundreds of moles per liter are typically used (*16*−*18*) to ensure that the starting solution is supersaturated.

The determination of C_{sat} itself has received less attention. It is important to quantify C_{sat}, as it represents the "safe" limit of the Aβ concentration, below which no aggregation can occur. If the C_{sat} measured *in vitro* deviates significantly from the estimated range of physiological concentrations, it may indicate the presence of physiological factors that can have a profound effect on the pathology. Even for modeling nucleation-limited growth kinetics, it is crucial to measure

[†] S.M. is supported by a Wellcome Trust Senior Overseas Research Fellowship in Biomedical Sciences in India (05995/Z/99/Z/HH/KO). P.S. and K.G. acknowledge partial support from the Kanwal Rekhi Scholarship of the TIFR Endowment Fund. This work is partially funded by the Picower Foundation.

* To whom correspondence should be addressed. E-mail: maiti@tifr.res.in.

[‡] Tata Institute of Fundamental Research.

[§] North Shore/LIJ Research Institute.

[1] Abbreviations: AD, Alzheimer's disease; Aβ, amyloid β peptide; $A\beta_{1-40}$, amyloid β peptide with amino acid residues 1−40; Rh-Lys-$A\beta_{1-40}$, $A\beta_{1-40}$ labeled with rhodamine at the N-terminus through a lysine; PBS, phosphate-buffered saline; CSF, cerebro spinal fluid; C_{sat}, saturation concentration; FCS, fluorescence correlation spectroscopy; MEMFCS, maximum entropy method-based FCS analysis routine; Tyr10, tyrosine at position 10 in the amino acid sequence; HPLC, high-performance liquid chromatography; MALDI-TOF, matrix-assisted laser desorption ionization time-of-flight; NA, numerical aperture.

10.1021/bi0341410 CCC: $25.00
Published on Web 08/13/2003

the degree of supersaturation ($C_{initial}/C_{sat}$) in the solution that is being studied. Also, C_{sat} provides a convenient benchmark for assaying the effect of an external agent, such as a metal ion, on Aβ aggregation. Different metal ions are believed to play a role in the pathology of AD (*19*−*21*), and it is important to understand whether they act by modulating the kinetic barriers or by actively altering the C_{sat}.

However, determination of C_{sat} has proven to be difficult. Many proteins and peptides do not exhibit a very well characterized C_{sat}, even in absence of obvious heterogeneity (*22*). Further, it is generally difficult to establish that a measured value represents the true thermodynamic solubility and not merely the apparent solubility of a quasi-stable state. In dynamic light scattering measurements at acidic pH, 25 μM is the lowest concentration at which Aβ aggregation is reported (*16*). With different methods, Aβ solubility has been measured to be 35 μM (*23*) at pH 7.4, and 6−9 μM (*24*) at pH 7.4. Together, all the results give an estimate for the saturation concentration of Aβ in the range of 6−40 μM at physiological pH (*25*). However, in the presence of cortical Aβ plaques or plaque-rich tissue homogenates, Aβ deposition is observed even at nanomolar concentrations (*26*). Thus, there appears to be a difference of almost 3 orders of magnitude in Aβ solubility between measurements performed in the presence and absence of diseased brain tissue. It is important to determine if this discrepancy is real and, if so, whether it signifies a difference in the kinetics of aggregation, or a true difference in the thermodynamic solubility in the two cases.

Ideally, a sensitive determination of Aβ concentration from a supersaturated solution that has stopped precipitating would yield C_{sat}. However, it is often not possible to know whether the precipitation has truly ceased, or whether it has merely become slow due to the presence of a kinetic trap or barrier. A more sensitive measurement would be to follow the size distribution of Aβ in the solution phase. When a supersaturated solution reaches thermodynamic equilibrium, not only does the precipitation cease but the size distribution in the solution phase also becomes stationary and independent of the starting solute concentration.

Here we use fluorescence of the single tyrosine residue in Aβ_{1-40}, Tyr10, for sensitive concentration determination of Aβ in solution. Subsequent mass spectroscopy examines the chemical identity of the components present in the supernatant and in the precipitate. We use fluorescence correlation spectroscopy (FCS) (*27*−*35*) to measure the size distribution of Aβ particles (partially labeled with rhodamine). FCS can measure the size of Aβ monomers as well as small and/or large aggregates simultaneously, has the capability to interrogate very low (nanomolar) to very high protein concentrations (using partial fluorescent labeling), and has a time resolution (for consecutive measurements) on the order of 1 min. Reisner and co-workers (*36*) have used FCS to show the presence of aggregated amyloid β peptide in the cerebro spinal fluid of an Alzheimer's patient but have not presented a particle size distribution. Rigler and co-workers have studied the aggregation of amyloid β peptide using FCS (*37*) where they have seen formation of aggregates at and above a concentration of 50 μM. However, so far FCS has seen limited use in Aβ aggregation, as it is difficult to interpret the data obtained from FCS when a multitude of diffusing species, varying in size by orders of magnitude, are present. Parameters such as diffusion constants (and hence size) are obtained from FCS data by fitting it to an appropriate model. A typical FCS data analysis algorithm interprets the FCS data in terms of a few diffusing components. These analysis methods are not very appropriate for highly heterogeneous systems such as an aggregating solution. Even if the data obtained from such a system can be adequately fit by a small number of diffusing components, this often leads to an unphysical and restricted description of the real system that is being studied. We have used a maximum entropy method-based analysis algorithm, MEM-FCS (*38*), to analyze the FCS data obtained from the study of amyloid β peptide aggregation. This method interprets the data in terms of the maximum number of diffusing components consistent with the data and thereby minimizes the possibility of overinterpretation in the case of highly heterogeneous systems.

In this article, we report the "saturation concentration" (C_{sat}) for Aβ_{1-40} at physiological pH as measured by fluorimetry. With FCS, we then measure the size distribution of the solution phase (after the apparent completion of the precipitation), both as a function of time and as a function of initial Aβ_{1-40} concentration. Finally, we quantitatively determine the effect of metal ions and coprecipitants such as Aβ_{1-42} on the measured C_{sat} under physiological conditions.

THEORY

Precipitation from a Supersaturated Solution. The supersaturation ratio (S) is defined as the ratio of the initial solute concentration (C_0) to the saturation concentration (C_{sat}) of the solute at a given temperature. When $S < 1$, there will not be any precipitation and the final concentration (C_f) of the solution is expected to be the same as the initial concentration. When $S > 1$, precipitation occurs until the saturation concentration is reached, and given sufficient time, the final concentration C_f of the solution equals C_{sat}. If the specimen contains an insoluble fraction f, which precipitates quickly and does not redissolve appreciably, then

$$C_f = (1 - f)C_0 \text{ for } (1 - f)C_0 \leq C_{sat} \Rightarrow \frac{C_0}{C_f} = \frac{1}{1 - f} \quad (1)$$

and

$$C_f = C_{sat} \text{ for } (1 - f)C_0 \geq C_{sat} \Rightarrow \frac{C_0}{C_f} = \frac{C_0}{C_{sat}} \quad (2)$$

So a plot of C_0/C_f versus C_0 would consist of two linear segments, one constant with a value of $1/(1 - f)$ for $C_0 \leq C_{sat}/(1 - f)$ and a line with a slope of $1/C_{sat}$ for $C_0 \geq C_{sat}/(1 - f)$. These two line segments meet at

$$C_0^* = \frac{C_{sat}}{1 - f} \quad (3)$$

Values of f and C_0^* can be obtained from the plot and can be used to obtain a value of C_{sat} from eq 3.

Fluorescence Correlation Spectroscopy (FCS). FCS measures spontaneous concentration fluctuations arising from the diffusive motion of single molecules in a small, optically defined, open probe volume using fluorescence detection.

The time scale of this fluctuation is related to diffusion. The characteristic residence time τ_D of a molecule in the probe volume is proportional to its hydrodynamic radius. The measured variable for FCS experiments is the temporal autocorrelation $G(\tau)$ of the fluorescence fluctuation, which is defined as

$$G(\tau) = \frac{\langle \delta F(t+\tau)\, \delta F(t) \rangle}{\langle F(t) \rangle^2} \quad (4)$$

where $\delta F(t)$ is the fluctuation in fluorescence at time t over the average fluorescence $\langle F(t) \rangle$. $G(\tau)$ is related to τ_D through the dimensions of the probe volume. When a laser beam with a Gaussian beam profile is used for excitation and the fluorescence is collected through a "confocal" pinhole, the probe volume generated can be described to a good approximation by a three-dimensional Gaussian function. If r and l are the characteristic radial and axial dimensions of the volume, respectively (i.e., where the Gaussian function drops to $1/e^2$ of its value at the maximum), $G(\tau)$ for a solution with n noninteracting fluorescent species is given by

$$G(\tau) = \sum_{i=1}^{n} b_i \left(\frac{1}{1 + \frac{\tau}{\tau_{D_i}}} \right) \left[\frac{1}{1 + \left(\frac{r}{l}\right)^2 \frac{\tau}{\tau_{D_i}}} \right]^{1/2} \quad (5)$$

Here

$$\tau_{D_i} = \frac{r^2}{4D_i} \quad (6)$$

where D_i values are the n different values of diffusion constants and b_i values are the relative weights of these components (*35*, *38*).

Obtaining the Size Distribution from FCS Data. Conventional models used to fit FCS data assume a small number of discrete diffusing species and are adequate for describing simple systems with limited heterogeneity. For extracting physically meaningful inferences from our FCS data on Aβ aggregation, a maximum entropy method-based analysis algorithm (MEMFCS) has been developed (*38*). MEMFCS interprets the data in terms of a quasi-continuous distribution of particle sizes and yields the *widest* possible size distribution that is consistent with the data. FCS results included in this article use this data analysis algorithm to achieve a bias-free interpretation of the data.

MATERIALS AND METHODS

Materials. Synthetic amyloid β peptide Aβ_{1-40} and rhodamine-labeled Aβ_{1-40} (labeled at the N-terminus through a lysine, Rh-Lys-Aβ_{1-40}) were purchased from Anaspec Inc. (San Jose, CA). The labeled peptide was purified using HPLC (protein and peptide C4 reversed phase column, pore size of 300 Å, column length of 250 mm, from Vydac, Hesperia, CA), and the purity was further verified to be >95% using mass spectrometry. Rh-Lys-Aβ_{1-40} was used for the experiments as a fluorescent probe molecule for FCS (at a ratio of approximately 1:1000 to unlabeled Aβ). Buffer salts were purchased from SD Fine Chemicals. Buffers used for FCS experiments were recrystallized twice from distilled water to make them free from fluorescent impurities. $MgCl_2$, $CaCl_2$, and $ZnCl_2$ salts were purchased from Qualigens.

Methods. Steady state fluorescence experiments were performed in a SPEX-FluoroMax-3 spectrometer (Jobin Yvon). Mass measurements were performed with a MALDI-TOF mass spectrometer (Micromass) in the linear data acquisition mode. For mass spectroscopy, the sample concentration was typically kept between 1 and 5 μM. The samples were prepared in 30% acetonitrile, 70% water, and 0.1% trifluoroacetic acid, and were mixed with α-cyano-4-hydroxycinnamic acid matrix in a 1:1 (v/v) proportion for the set of experiments described here. Bovine insulin was used for calibrating the mass spectrum.

FCS experiments were performed in a home-built spectrometer with single-photon excitation. The MEMFCS fitting routine (*38*) was used to obtain size distributions from FCS data. The instrument has been described elsewhere (*35*). In short, the experimental setup consisted of a high-numerical aperture objective lens (40×, 1.3 NA, oil immersion, Carl Zeiss, Jena, Germany), which focuses a continuous wave green He:Ne laser (1.2 mW at 543.5 nm, Jain Laser Technology) beam into the sample. The laser power at the objective back aperture was kept typically below 100 μW. The beam waist in the objective focal plane was a fraction of a micrometer for most of these experiments. Fluorescence was collected through the same microscope objective, separated from the excitation light by both a dichroic mirror (560DCLP, Chroma Inc.) and an emission filter (585DF40, Chroma Inc.), and focused with an achromat lens ($F = 150$ mm, Newport) onto a multimode fiber (50 μm core diameter, Newport). The other end of the fiber was connected to a fiber-coupled APD detector (SPCM-AQR-150, Perkin-Elmer). The detector signal was then processed with an autocorrelator card (ALV5000). The correlation decay traces were then fit with eq 5 using the MEMFCS algorithm.

RESULTS

Fluorimetric Determination of the Saturation Concentration of Aβ_{1-40}. Aβ_{1-40} solutions at different concentrations ranging from 900 nM to 170 μM were made in PBS buffer (pH 7.4). Three different solutions at 120, 150, and 170 μM were prepared by weighing lyophilized Aβ_{1-40}. Lower-concentration solutions were prepared by serial dilution from these three samples. Initial concentrations were accurate to 5% of the measured value. Total protein contents in these samples were measured by Tyr10 fluorescence of Aβ_{1-40} at the initial time. Fluorescence from a freshly prepared tyrosine solution was used to calibrate the signal in terms of a "tyrosine equivalence" in fluorescence. This accounted for any day-to-day variation in instrumental sensitivity. Tyrosine in Aβ_{1-40} was quenched, and its fluorescence was ~31% of that obtained from free tyrosine in PBS buffer (pH 7.4). The inset of Figure 1 shows the tyrosine (Tyr10) fluorescence of Aβ_{1-40} at different starting protein concentrations (C_0) at the initial time (○). Initial time point measurements were taken immediately after the samples were prepared. Subsequently, all these samples were kept in the dark at room temperature for 2 days to allow precipitation. After 2 days, each sample was centrifuged at 2000*g* for 20 min and tyrosine fluorescence was recorded from the supernatant. The inset of Figure 1 (□) shows the supernatant fluorescence after

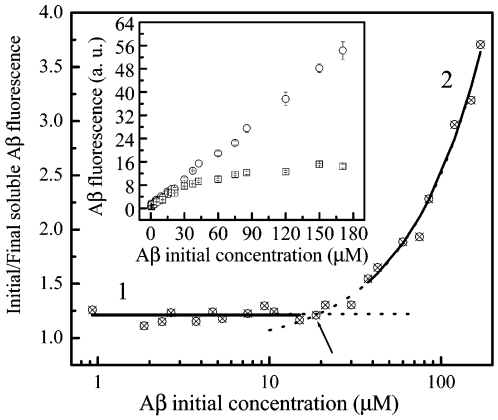

FIGURE 1: Aβ_{1-40} fluorescence as a function of initial concentration. The ratio of initial to final (day 2) fluorescence of the soluble fraction of Aβ_{1-40} (C_0/C_f) as a function of initial concentration C_0 (⊗). A fit of the lower concentration points with eq 1 (solid line 1 with a slope of 0) and a fit of the higher concentration points with eq 2 (solid line 2) when extrapolated meet at 18.8 μM (point marked with an arrow). The intersection point of these two lines yields a C_{sat} value of 15.5 ± 1 μM using eq 3. The inset shows the Tyr10 fluorescence of Aβ_{1-40} as a function of starting concentration C_0 at initial time (○) and after 2 days (□) (same data as the main figure). Error bars denote the standard deviation of six measurements.

2 days (C_f) for different starting concentrations of Aβ_{1-40}. While at smaller concentrations C_f remains proportional to C_0, in the higher concentration range C_f attains a constant value. Intermediate concentrations show a gradual changeover between these two regimes. No further precipitation is observed when the samples are kept for longer times (up to an additional 3 days, data not shown). Figure 1 shows the same data presented in the inset in terms of C_0/C_f versus C_0 (⊗). The transition becomes more apparent in this plot. A constant fractional loss (f) for all the samples at a C_0 of <20 μM is observed. A linear fit to the lower concentration points (up to 15 μM) with a slope of 0 yields a value of 0.18 ± 0.01 for the constant fractional loss f. A fit of the higher concentration points (>36 μM) using eq 2 yields an intersection point with the lower concentration region fit at 18.8 μM, which yields a value of 15.5 ± 1 μM for C_{sat} of Aβ_{1-40} peptide at pH 7.4 (using eq 3).

The supernatant obtained from the 100 μM Aβ_{1-40} sample by centrifuging it at 2000g for 20 min was heated to 68 °C for 1 h. The sample was then brought back slowly to room temperature, and the fluorescence of the supernatant obtained after a 2000g spin for 20 min was measured. The solubility of the Aβ_{1-40} sample was reduced by 11.5%.

Mass Spectroscopic Characterization of the Supernatant and the Precipitate. Small portions of the supernatant as well as the precipitate from the 2-day-old Aβ_{1-40} sample (initial concentration of 100 μM), separated by centrifuging the sample at 2000g for 20 min, were characterized using MALDI-TOF mass spectroscopy. Figure 2 shows the mass spectrum obtained with the supernatant (A) and with the precipitate (B). Both traces exhibit a mass peak at ~4331 Da indicating the presence of Aβ_{1-40} in them as the predominant peptide.

Time Dependence of the Size Distribution of Aβ_{1-40} in Solution. Aβ_{1-40} samples (158 μM) in PBS buffer (pH 7.4) were prepared and kept at room temperature and in the dark for different periods of time. All the specimens contained

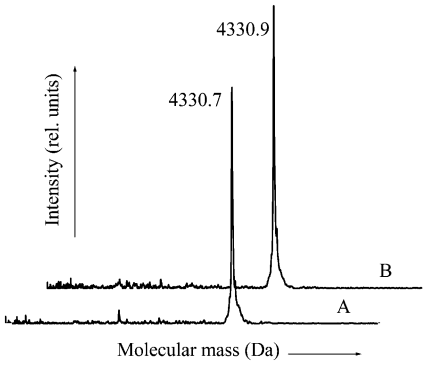

FIGURE 2: Mass spectra obtained with Aβ_{1-40}. Mass spectra of the supernatant (A) and the precipitate (B) obtained from a 100 μM Aβ_{1-40} sample, after incubation for 2 days at room temperature.

~100 nM Rh-Lys-Aβ_{1-40} as a probe for FCS measurement. Before the measurement, all specimens were centrifuged at 2000g for 10 min. Figure 3A shows the supernatant rhodamine fluorescence (△) for specimens kept for different periods of time. Supernatant fluorescence decreases with time and finally reaches a constant value after 940 min. A 10 μM Aβ_{1-40} sample with ~100 nM Rh-Lys-Aβ_{1-40} was used as a control for this set of experiments. Circles in Figure 3A represent the supernatant fluorescence recorded with the control, each value multiplied by a factor of 2.5 for convenience of representation. The supernatant fluorescence of the control does not change with time. FCS measurements were performed with the supernatants at each time point, and the autocorrelation traces that were obtained are presented in Figure 3B. The autocorrelation traces obtained with 158 μM Aβ_{1-40} vary with time initially [45 min in Figure 3B (- - -), 230 min in Figure 3B (-•-), and 1300 min in Figure 3B (—)]. However, the autocorrelation trace stops changing after 1300 min, as shown by the nearly overlapping autocorrelation traces at 1300 min [Figure 3B (—)] and 2400 min [Figure 3B (•••)]. In contrast, the autocorrelation trace obtained from the 10 μM Aβ_{1-40} control sample does not change with time. The autocorrelation trace was obtained at 45 min [Figure 3B (○)] and overlaps that obtained at 1300 min [Figure 3B (-••-)]. Figure 3C shows the different size distributions obtained from FCS data as a function of time using MEMFCS analysis: rhodamine B (C1); 10 μM Aβ_{1-40} after 1300 min (C2); and 158 μM Aβ_{1-40} after 45 min (C3), after 230 min (C4), after 1300 min (C5), and after 2400 min (C6). For the 158 μM Aβ_{1-40} sample, initially the soluble fraction contains a monomer/dimer-like species (2.5 times the diffusion time of rhodamine B) and also soluble oligomeric species. With time the oligomeric peak becomes more pronounced, but the distribution does not change after 1300 min as is evident from the distributions in panels C5 and C6 of Figure 3. At both these time points, the distributions show a peak around 1.5 ms (24 times greater than the diffusion time of rhodamine B).

Initial Concentration Dependence of the Final Size Distribution. Aβ_{1-40} peptide solutions at different concentrations (175, 155, 126, and 11.4 μM) were prepared by serial dilution from a concentrated (200 μM) stock solution containing ~100 nM Rh-Lys-Aβ_{1-40} as the fluorescent probe. All the samples were prepared in <1 min before substantial aggregation could take place. These solutions were incubated at room temperature, in the dark, to allow aggregation. After

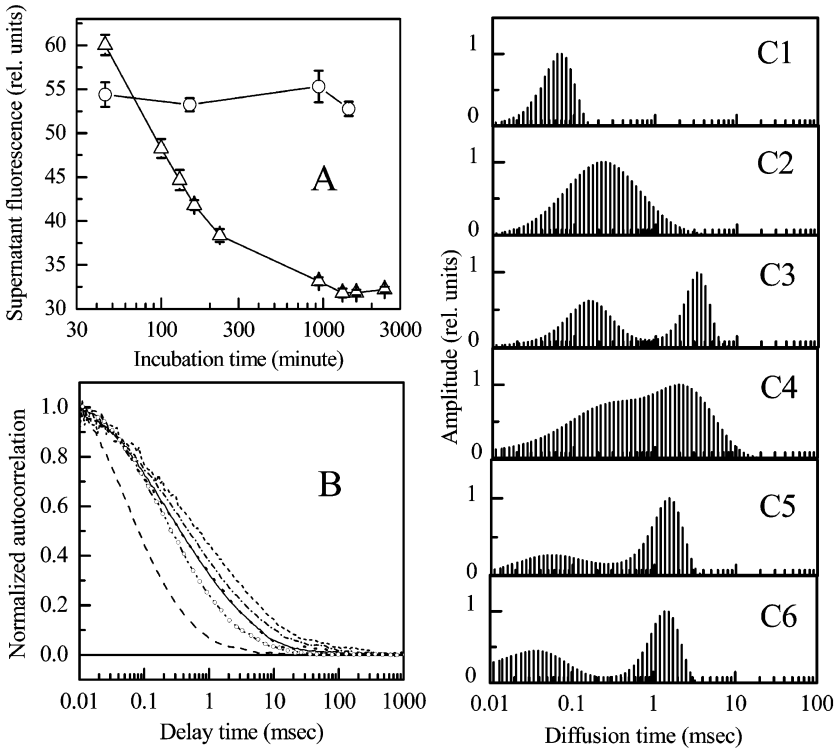

FIGURE 3: Size distributions of the soluble fraction of Aβ_{1-40} at different incubation times. (A) Supernatant fluorescence from 158 μM (△) and 10 μM Aβ_{1-40} (○) at different incubation times. Both the samples contain ~100 nM Rh-Lys-Aβ_{1-40}. (B) Autocorrelation traces obtained with rhodamine B (— — —), 158 μM Aβ_{1-40} supernatants at different incubation times [45 (- - -), 230 (-·-), 1300 (—), and 2400 min (···)], and 10 μM Aβ_{1-40} at different incubation times [45 (○) and 1300 min (-···)]. (C) Size distribution obtained from MEMFCS analysis of autocorrelation traces presented in panel B: rhodamine B (C1), 10 μM Aβ_{1-40} after 1300 min (C2), and 158 μM Aβ_{1-40} after 45 (C3), 230 (C4), 1300 (C5), and 2400 min (C6).

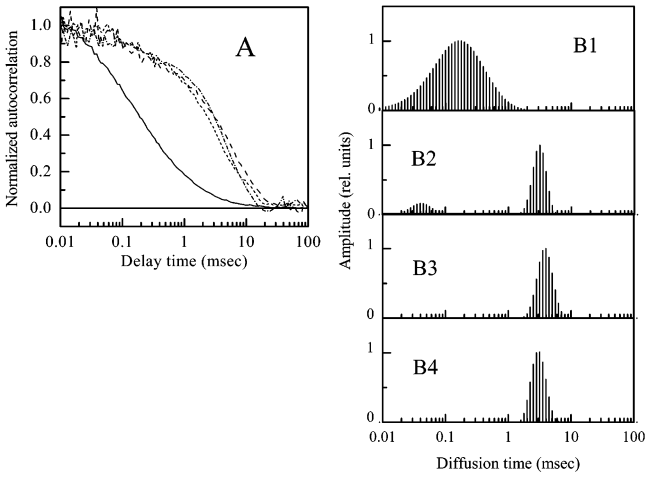

FIGURE 4: Size distribution of the soluble fraction of Aβ_{1-40} at different starting concentrations. (A) Autocorrelation traces obtained with Aβ_{1-40} remaining in solution after 2 days at different starting concentrations: 11.4 (—), 126 (- - -), 155 (— — —), and 175 μM (-·-). (B) Size distribution obtained with MEMFCS analysis of the autocorrelation curves presented in panel A: Aβ_{1-40} samples with initial concentrations of 11.4 (B1), 126 (B2), 155 (B3), and 175 μM (B4).

48 h, the soluble fraction from each sample was separated by centrifugation at 2000*g* for 20 min. The FCS data recorded at different starting concentrations are presented in Figure 4A. Rhodamine B was used for calibration (autocorrelation trace not shown). The autocorrelation traces recorded with a sample for which $C_0 < C_{sat}$ [Figure 4A (—), 11.4 μM] are different from those for which $C_0 > C_{sat}$ [Figure 4A, 126 μM (- - -), 155 μM (— — —), and 175 μM (-·-)]. The data that were obtained were analyzed using the MEMFCS fitting routine. The size distributions obtained from fitting the autocorrelation functions are shown in Figure 4B. The distributions obtained at starting concentrations below the saturation concentration (11.4 μM) exhibit a peak diffusion time of ~200 μs (panel B1 of Figure 4), which is ~2.1 times greater than that of the peak obtained with rhodamine B (peak at 95 μs). On the other hand, the distributions obtained with the supernatant of the solutions whose starting concentrations are above the saturation concentration of Aβ_{1-40} (126, 155, and 175 μM) show the presence of soluble oligomers with peak diffusion times in the range of 3.1−4.0 ms (panels B2−B4 of Figure 4, respectively). The size distributions obtained with the supernatant for different starting concentrations where $C_0 > C_{sat}$ are very similar. Variation of the position of the peak does not show any trend vis-à-vis the starting concentration.

Effect of Ca^{2+}, Mg^{2+}, and Zn^{2+} on C_{sat}. We prepared near-saturating concentrations of these ions (2 mM Mg^{2+}, 2.5 μM Ca^{2+}, and 4 μM Zn^{2+}) in PBS (pH 7.4) and measured C_{sat} in these buffers. All these samples were kept at room temperature and in the dark for 24 h. Each sample was then centrifuged at 2000*g* (for 20 min) to separate the precipitate from the supernatant, and fluorimetric concentration measurements were performed with the supernatant. All of the ions that were investigated were observed to lower C_{sat}, but by relatively small amounts (6−11%; see Table 1).

DISCUSSION

Tyrosine Fluorescence Measures the Soluble Aβ Concentration. Tyrosine (Tyr10) fluorescence from Aβ_{1-40} presents

Table 1: Relative Solubility of $A\beta_{1-40}$ in the Presence of Different Divalent Metal Ions in PBS Buffer (pH 7.4)

	Ca^{2+}	Mg^{2+}	Zn^{2+}
ion concentration	2.5 μM	2 mM	4 μM
percent solubility reduction for $A\beta_{1-40}$	6.9%	6.3%	10.8%

a sensitive yet robust measure of protein concentration. The inset of Figure 1 shows that at the initial time ($t = 0$), Aβ fluorescence in tyrosine equivalence remains linear with Aβ concentrations (○), showing that concentration- or aggregation-dependent artifacts are negligible over the concentration range that was studied. Tyrosine in $A\beta_{1-40}$ exhibits ~31% of the fluorescence intensity of free tyrosine in PBS buffer. This is not surprising, as the presence of other residues around the tyrosine in Aβ can quench its fluorescence.

A Saturation Behavior Is Observed. At low concentrations, the final fluorescence (at $t = 2$ days) remains proportional to the initial Aβ concentration [Figure 1 inset (□)]. At high concentrations, the final fluorescence attains a constant value [Figure 1 inset (□)]. This is the hallmark of a supersaturated solution attaining thermodynamic equilibrium. But even at very low concentrations (~1 μM) there is some loss (~18%) of soluble protein over the course of 2 days. The amount of this loss is independent of the starting protein concentration as is obvious from Figure 1. This constant fractional loss is attributed to an insoluble fraction of the lyophilized $A\beta_{1-40}$. The existence of an insoluble fraction does not alter the theoretical description of the aggregation process. These may be large particles that have been produced and/or retained by the lyophilization process. Such insoluble fractions are routinely observed in other experiments involving Aβ (*16*, *18*, *24*).

We observed that the transition to supersaturation is not very sharp. The data indicate that there is no precipitation below 14 μM, whereas if the initial concentration of the solution is much higher than the saturation concentration, the final solubility becomes ~36 μM in PBS buffer (pH 7.4). This lack of sharpness in the concentration region near the saturation concentration suggests possible heterogeneity in the solution (*22*). If the insoluble fraction is taken into account (Figure 1), the saturation concentration manifests itself more clearly. The two-segment linear fits, based on eqs 1 and 2, describe the data well (Figure 1). The value of the insoluble fraction is found to be 0.18 ± 0.01. The C_{sat} value obtained from the intersection point of the fits using eq 3 is 18.8 μM. Our primary focus here is the lower limit of the Aβ solubility, and we take 15.5 ± 1 μM to be the observed saturation concentration of $A\beta_{1-40}$ in PBS buffer (pH 7.4).

The Supernatant and the Precipitate Contain Chemically Indistinguishable $A\beta_{1-40}$. A tyrosine-like impurity (for instance, a fragment of Aβ) may affect our solution phase Aβ estimates. In an extreme case, the entire fluorescence signal in the solution phase may come from such an impurity, with the actual $A\beta_{1-40}$ completely precipitated. Mass spectrometric characterization of the supernatant and the precipitates obtained from a 100 μM $A\beta_{1-40}$ sample (Figure 2) shows $A\beta_{1-40}$ (formula weight of 4331) is the major component above 700 Da in both. This establishes that $A\beta_{1-40}$ is present in the supernatant, and it coexists with precipitated $A\beta_{1-40}$ when saturation is observed.

Is the Observed C_{sat} the True Thermodynamic C_{sat}? Before we accept the observed C_{sat} as the thermodynamic C_{sat}, we need to verify that no further precipitation occurs even if the duration of the experiment is increased. However, it is not possible to continue the experiment indefinitely. The size distribution of the Aβ particles in the solution phase can serve as a sensitive indicator of the completion of precipitation. A development of the size distribution, even when no precipitation is observed, would indicate that equilibrium has not yet been attained. Kinetic barriers (e.g., requirement for nucleation or a conformational transition) may make the size distribution apparently stationary, but the kinetics would be sensitive to the variation of initial concentrations. Kinetics of barrier crossing are also expected to be strongly affected by a variation in temperature.

The Aβ Size Distribution in the Solution Phase Becomes Independent of Time and Initial Concentration. After 1300 min, the fluorescence of the supernatant (obtained from an initial concentration C_0 of 158 μM) does not change any further with time [Figure 3A (△)]. The size distributions obtained at and after this time are also similar (panels C5 and C6, respectively, of Figure 2). This indicates that the same species are present in the sample at and after 1300 min, indicating a completion of the aggregation process.

The size distributions obtained after 2 days from the soluble fractions depend strongly on whether the starting concentration is above or below the saturation concentration. However, the size distributions obtained with different starting concentrations above the saturation concentration of $A\beta_{1-40}$ are very similar (panels B2−B4 of Figure 4). The small variations in the peak positions and the widths are not deemed to be significant for a data set analyzed with MEMFCS, as this algorithm actively widens the distribution as much as the errors allow. Moreover, the small variation does not correlate with the initial concentration.

Panels C5 and C6 of Figure 3 and also panels B2−B4 of Figure 4 show peaks at large diffusion times. It has been recently shown that the diffusion time distribution derived from single-photon-excited FCS experiments can have some artifacts (*39*). However, we have repeated some of these experiments with two-photon-excited FCS, and the size distributions obtained are very similar (data not shown). This peak thus indicates the presence of relatively large soluble oligomers in the saturated solution at equilibrium. We note that oligomers have been suggested to be the major toxic agents in Alzheimer's disease (*40*).

Metal Ions at Low Concentrations Do Not Have a Large Effect on the Observed C_{sat}. Metal ions are suspected to play a role in Aβ precipitation *in vivo* (*19*−*21*, *41*). They can affect precipitation either by speeding the kinetics or by lowering the C_{sat} of Aβ. In cerebro spinal fluid, Ca^{2+}, Mg^{2+}, and Zn^{2+} are present and hence can affect Aβ solubility. In addition to that, Zn^{2+} is found in brain plaques and is believed to promote *in vivo* Aβ aggregation. We have investigated the effect of three different divalent metal ions, viz. Ca^{2+}, Mg^{2+}, and Zn^{2+}, on Aβ aggregation. The solubilities of metal ions in PBS buffer are calculated from the metal ion phosphate solubility products (*42*). The theoretically obtained solubility limits for these metal ions are verified experimentally by monitoring the Rayleigh scattering signal at 500 nm in a fluorimeter. At levels close to their solubility limits in PBS buffer (pH 7.4), these metal ions only reduce

the C_{sat} value by 6−11% (Table 1). We note that these ions are not buffered in the solution, and their concentration may change with Aβ aggregation. Even if the *in vivo* concentrations of these ions vary, it appears to be unlikely that they would change C_{sat} by orders of magnitude. A variation of pH cannot effect such a large change either [percent aggregation of Aβ_{1-40} changes by a factor of <5 with a pH change in the range of pH 3−8 (*43*)].

Incubation at Higher Temperatures Does Not Appreciably Alter the Observed C_{sat}. If a kinetic barrier stalls precipitation, incubation at higher temperatures should markedly change precipitation. Yet incubation of the supernatant of a 100 μM Aβ sample (after precipitation for 2 days) at 68 °C for 1 h changes the soluble concentration by <12%. When the possibility that thermally activated chemical processes may also lower the fluorescence is considered, the actual extent of precipitation may be even lower.

The Observed C_{sat} Is in Sharp Contrast with in Vivo Estimates. Given that (a) the precipitation is complete in 2 days and shows a clear signal of saturation, (b) the solution phase and the precipitate contain chemically identical Aβ molecules, (c) the size distribution in the solution phase is stationary in time and independent of initial concentration (even in the presence of bigger aggregates that may serve as nuclei), and (d) incubation at higher temperature does not lead to appreciable additional precipitation, we conclude that C_{sat} measured by us is the true thermodynamic saturation concentration. We also note that none of the reported *in vitro* experiments have observed aggregation at a concentration much lower than 10 μM. The *in vitro* concentration of Aβ even in a diseased brain is estimated to be in the nanomolar range (*6*, *7*, *26*). In presence of plaque-rich tissue homogenates, aggregation of Aβ_{1-40} is reported even in the nanomolar concentration range (*26*). Since no aggregation can occur at a starting concentration that is lower than the thermodynamic saturation concentration, our measurements show that the solubility of Aβ *in vivo* is orders of magnitude lower than that *in vitro*. Small differences in metal ion concentrations, temperature, pH, ionic strength, etc., between *in vitro* and the actual *in vivo* conditions are unlikely to bridge this large gap. Aβ_{1-42} is known to coprecipitate with Aβ_{1-40} in physiological plaques. However, the saturation concentration of Aβ_{1-42} by itself and that of an equimolar mixture of Aβ_{1-40} and Aβ_{1-42} are both $\gtrsim$2 μM (data not shown).

It therefore appears likely that some other coprecipitant(s) drives the C_{sat} for Aβ *in vivo* to a value which is lower by orders of magnitude. The key to dealing with Aβ aggregation *in vivo* may lie in understanding these agents.

ACKNOWLEDGMENT

We thank Mrs. Geetanjali R. Dhotre for her help in acquiring the mass spectra and Radha Desai for her help in the metal ion scattering studies. We thank Prof. David B. Teplow for his kind gift of Aβ_{1-42}.

REFERENCES

1. Smith, M. A. (1998) Alzheimer's Disease, in *International Review of Neurobiology*, pp 1−54, Academic Press, New York.
2. Selkoe, D. J. (1991) The molecular pathology of Alzheimer's disease, *Neuron 6*, 487−498.
3. Selkoe, D. J. (2001) Alzheimer's disease: genes, proteins and therapy, *Physiol. Rev. 81*, 741−766.
4. Teplow, D. B. (1998) Structural and kinetic features of amyloid β protein fibrillogenesis, *Amyloid 5*, 121−142.
5. Haass, C., Schlossmacher, M. G., Hung, A. Y., Vigo-Pelfrey, C., Mellon, A., Ostaszewski, B. L., Lieberburg, I., Koo, E. H., Schenk, D., and Teplow, D. B. (1992) Amyloid β-peptide is produced by cultured cells during normal metabolism, *Nature 359*, 322−325.
6. Shoji, M., Golde, T. E., Ghiso, J., Cheung, T. T., Estus, S., Shaffer, L. M., Cai, X. D., McKay, D. M., Tintner, R., Frangione, B., and Younkin, S. G. (1992) Production of the Alzheimer amyloid β protein by normal proteolytic processing, *Science 258*, 126−129.
7. Seubert, P., Vigo-Pelfrey, C., Esch, F., Lee, M., Dovey, H., Davis, D., Sinha, S., Schlossmacher, M. G., Whaley, J., Swindlehurst, C., McCormack, R., Wolfert, R., Selkoe, D. J., Lieberburg, I., and Schenk, D. (1992) Isolation and quantification of soluble Alzheimer's β-peptide from biological fluids, *Nature 359*, 325−327.
8. Petkova, A. T., Yoshitaka, I., Balbach, J. J., Antzutkin, O. N., Leapman, R. D., Delaglio, F., and Tycko, R. (2002) A structural model for Alzheimer's β-amyloid fibrils based on experimental constraints from solid-state NMR, *Proc. Natl. Acad. Sci. U.S.A. 99*, 16742−16747.
9. Thompson, L. K. (2003) Unraveling the secrets of Alzheimer's β-amyloid fibrils, *Proc. Natl. Acad. Sci. U.S.A. 100*, 383−385.
10. Pike, C. J., Walencewicz, A. J., Glabe, C. G., and Cotman, C. W. (1991) In vitro aging of β-amyloid protein causes peptide aggregation and neurotoxicity, *Brain Res. 563*, 311−314.
11. Pike, C. J., Burdick, D., Walencewicz, A. J., Glabe, C. G., and Cotman, C. W. (1993) Neurodegeneration induced by β-amyloid peptides in vitro: The role of peptide assembly state, *J. Neurosci. 13*, 1676−1687.
12. Hardy, J. A., and Higgins, G. A. (1992) Alzheimer's disease: the amyloid cascade hypothesis, *Science 256*, 184−185.
13. Jarrett, J. T., and Lansbury, P. T., Jr. (1993) Seeding "one-dimensional crystallization" of amyloid: A pathogenic mechanism in Alzheimer's disease and scrapie? *Cell 73*, 1055−1058.
14. Hofrichter, J., Ross, P. D., and Eaton, W. A. (1974) Kinetics and mechanism of deoxyhemoglobin S gelation: A new approach to understanding sickle cell disease, *Proc. Natl. Acad. Sci. U.S.A. 71*, 4864−4868.
15. Perutz, M. F., and Windle, A. H. (2001) Cause of neural death in neurodegenerative diseases attributable to expansion of glutamine repeats, *Nature 412*, 143−144.
16. Lomakin, A., Chung, D. S., Benedek, G. B., Kirschner, D. A., and Teplow, D. B. (1996) On the nucleation and growth of amyloid β-protein fibrils: Detection of nuclei and quantitation of rate constants, *Proc. Natl. Acad. Sci. U.S.A. 93*, 1125−1129.
17. Lomakin, A., Teplow, D. B., Kirschner, D. A., and Benedek, G. B. (1997) Kinetic theory of fibrillogenesis of amyloid β-protein, *Proc. Natl. Acad. Sci. U.S.A. 94*, 7942−7947.
18. Yong, W., Lomakin, A., Kirkitadze, M. D., Teplow, D. B., Chen, S.-H., and Benedek, G. B. (2002) Structure determination of micelle-like intermediates in amyloid β-protein fibril assembly by using small angle neutron scattering, *Proc. Natl. Acad. Sci. U.S.A. 99*, 150−154.
19. Atwood, C. S., Huang, X., Khatri, A., Scarpa, R. C., Kim, Y. S., Moir, R. D., Tanzi, R. E., Roher, A. E., and Bush, A. I. (2000) Copper catalyzed oxidation of Alzheimer Aβ, *Cell. Mol. Biol. 46*, 777−783.
20. Cuajungco, M. P., Goldstein, L. E., Nunomura, A., Smith, M. A., Lim, J. T., Atwood, C. S., Huang, X., Farrag, Y. W., Perry, G., and Bush, A. I. (2000) Evidence that the beta-amyloid plaques of Alzheimer's disease represent the redox-silencing and entombment of Aβ by zinc, *J. Biol. Chem. 275*, 19439−19442.
21. Huang, X., Atwood, C. S., Hartshorn, M. A., Multhaup, G., Goldstein, L. E., Scarpa, R. C., Cuajungco, M. P., Gray, D. N., Lim, J., Moir, R. D., Tanzi, R. E., and Bush, A. I. (1999) The Aβ peptide of Alzheimer's disease directly produces hydrogen peroxide through metal ion reduction, *Biochemistry 38*, 7609−7616.
22. Arakawa, T., and Timasheff, S. N. (1985) Theory of protein solubility, in *Methods of Enzymology*, Vol. 114, pp 49−77, Academic Press, New York.
23. Evans, K. C., Berger, E. P., Cho, C., Weisgraber, K. H., and Lansbury, P. T., Jr. (1995) Apolipoprotein E is a kinetic but not a thermodynamic inhibitor of amyloid formation: Implications for the pathogenesis and treatment of Alzheimer disease, *Proc. Natl. Acad. Sci. U.S.A. 92*, 763−767.

24. Jarrett, J. T., Berger, E. P., and Lansbury, P. T., Jr. (1993) The carboxy terminus of the beta amyloid protein is critical for the seeding of amyloid formation: implications for the pathogenesis of Alzheimer's disease, *Biochemistry 32*, 4693−4697.
25. Harper, J. D., and Lansbury, P. T., Jr. (1997) Models of amyloid seeding in Alzheimer's disease and scrapie: Mechanistic truths and physiological consequences of the time-dependent solubility of amyloid proteins, *Annu. Rev. Biochem. 66*, 385−407.
26. Esler, W. P., Stimson, E. R., Ghilardi, J. R., Vinters, H. V., Lee, J. P., Mantyh, P. W., and Maggio, J. E. (1996) In vitro growth of Alzheimer's disease β-amyloid plaques displays first-order kinetics, *Biochemistry 35*, 749−757.
27. Magde, D., Elson, E., and Webb, W. W. (1972) Thermodynamic fluctuation in a reaction system: measurement by fluorescence correlation spectroscopy, *Phys. Rev. Lett. 29*, 705−708.
28. Elson, E., and Magde, D. (1974) Fluorescence correlation spectroscopy: I. Conceptual basics and theory, *Biopolymers 13*, 1−27.
29. Magde, D., Elson, E., and Webb, W. W. (1974) Fluorescence correlation spectroscopy: II An experimental realization, *Biopolymers 13*, 29−61.
30. Eigen, M., and Rigler, R. (1994) Sorting single molecules: Application to diagnostics and evolutionary biotechnology, *Proc. Natl. Acad. Sci. U.S.A. 91*, 5740−5747.
31. Maiti, S., Haupts, U., and Webb, W. W. (1997) Fluorescence Correlation Spectroscopy: Diagnostics for sparse molecules, *Proc. Natl. Acad. Sci. U.S.A. 94*, 11753−11757.
32. Rigler, R., and Elson, E. S., Eds. (2000) Fluorescence correlation spectroscopy: Theory and application, *Springer Series in Chemical Physics*, Springer Press, Berlin.
33. Schwille, P. (2001) Fluorescence correlation spectroscopy and its potential for intracellular applications, *Cell Biochem. Biophys. 34*, 383−408.
34. Hess, S. T., Huang, S., Heikal, A. A., and Webb, W. W. (2002) Biological and chemical applications of fluorescence correlation spectroscopy: A review, *Biochemistry 41*, 697−705.
35. Sengupta, P., Balaji, J., and Maiti, S. (2002) Measuring diffusion in cell membranes by fluorescence correlation spectroscopy, *Methods 27*, 374−387.
36. Pitschke, M., Prior, R., Haupt, M., and Riesner, D. (1998) Detection of single amyloid beta protein aggregates in the cerebrospinal fluid of Alzheimer's patient by fluorescence correlation spectroscopy, *Nat. Med. 4*, 832−834.
37. Tjernberg, L. O., Pramanik, A., Bjorling, S., Thyberg, P., Thyberg, J., Nordstedt, C., Berndt, K. D., Terenius, L., and Rigler, R. (1999) Amyloid β-peptide polymerization studied using fluorescence correlation spectroscopy, *Chem. Biol. 6*, 53−62.
38. Sengupta, P., Garai, K., Balaji, J., Periasamy, N., and Maiti, S. (2003) Measuring size distribution in highly heterogeneous systems with fluorescence correlation spectroscopy, *Biophys. J. 84*, 1977−1984.
39. Hess, S. T., and Webb, W. W. (2002) Focal volume optics and experimental artifacts in confocal fluorescence correlation spectroscopy, *Biophys. J. 83*, 2300−2317.
40. Lashuel, H. A., Hartley, D., Petre, B. M., Walz, T., and Lansbury, P. T. (2002) Neurodegenerative disease: Amyloid pores from pathogenic mutations, *Nature 318*, 291.
41. Huang, X., Atwood, C. S., Moir, R. D., Hartshorn, M. A., Vonsattel, J.-P., Tanzi, R. E., and Bush, A. I. (1997) Zinc-induced Alzheimer's Aβ_{1-40} aggregation is mediated by conformational factors, *J. Biol. Chem. 272*, 26464−26470.
42. Lide, D. R. (1999−2000) *CRC Handbook of Chemistry and Physics*, CRC Press, Boca Raton, FL.
43. Wood, S. J., Maleeff, B., Hart, T., and Wetzel, R. (1996) Physical, morphological and functional differences between pH 5.8 and 7.4 aggregates of the Alzheimer's amyloid peptide Aβ, *J. Mol. Biol. 256*, 870−877.

BI0341410